

ARTICLE OPEN



BNIP3 phosphorylation by JNK1/2 promotes mitophagy via enhancing its stability under hypoxia

Yun-Ling He^{1,7}, Jian Li^{2,3,7}, Sheng-Hui Gong¹, Xiang Cheng¹, Ming Zhao¹, Yan Cao², Tong Zhao¹, Yong-Qi Zhao¹, Ming Fan^{1,4,5,6}, Hai-Tao Wu^{1,4}, Ling-Ling Zhu^{1,5} and Li-Ying Wu^{1,2}

© The Author(s) 2022

Mitophagy is an important metabolic mechanism that modulates mitochondrial quality and quantity by selectively removing damaged or unwanted mitochondria. BNIP3 (BCL2/adenovirus e1B 19 kDa protein interacting protein 3), a mitochondrial outer membrane protein, is a mitophagy receptor that mediates mitophagy under various stresses, particularly hypoxia, since BNIP3 is a hypoxia-responsive protein. However, the underlying mechanisms that regulate BNIP3 and thus mediate mitophagy under hypoxic conditions remain elusive. Here, we demonstrate that in hypoxia JNK1/2 (c-Jun N-terminal kinase 1/2) phosphorylates BNIP3 at Ser 60/Thr 66, which hampers proteasomal degradation of BNIP3 and drives mitophagy by facilitating the direct binding of BNIP3 to LC3 (microtubule-associated protein 1 light chain 3), while PP1/2A (protein phosphatase 1/2A) represses mitophagy by dephosphorylating BNIP3 and triggering its proteasomal degradation. These findings reveal the intrinsic mechanisms cells use to regulate mitophagy via the JNK1/2-BNIP3 pathway in response to hypoxia. Thus, the JNK1/2-BNIP3 signaling pathway strongly links mitophagy to hypoxia and may be a promising therapeutic target for hypoxia-related diseases.

Cell Death and Disease (2022)13:966; <https://doi.org/10.1038/s41419-022-05418-z>

INTRODUCTION

Under normal circumstances, functional mitochondria are energy factories that provide the cellular ATP required for cellular activities. However, under hypoxic conditions, mitochondria become sites where excessive reactive oxygen species (ROS) are generated, which in turn impairs mitochondrial function [1]. The damaged mitochondria usually release proteins that participate in regulation of apoptosis [2–4]. To defend against the harmful effects of dysfunctional mitochondria and maintain homeostasis, cells initiate protective mechanisms to compensate for damaged mitochondria prior to suffering harm. Mitophagy is recognized as a major protective mechanism by which dysfunctional mitochondria are cleared to enhance overall mitochondria quality and simultaneously provide rapid recycling of metabolites [5]. The mitophagy process is complicated and involves mitochondrial dynamics, recognition and labeling of target mitochondria, envelopment of mitochondria by autophagosomes, fusion of autophagosomes-lysosomes and degradation of mitochondria by proteases in lysosomes [3, 5, 6]. Among these processes, recognizing and labeling damaged or unwanted mitochondria is a crucial process, considering that mitophagy is one of selective autophagy.

Two crucial recognition signals are required for mitophagy in mammalian cells: ubiquitin (Ub)-adapter- and receptor-mediated mitochondrial conjunction with LC3 (microtubule-associated

protein 1 light chain 3) on the autophagosomes [7, 8]. Ubiquitin-adapter-mediated mitophagy is provoked by the classic PINK1 (PTEN-induced kinase 1) and E3 ubiquitin protein ligase Parkin pathway [9], and receptor-mediated mitophagy is initiated by several mitochondrial outer membrane proteins: the BH3-only proteins BNIP3 (BCL2/adenovirus e1B 19 kDa protein interacting protein 3) and BNIP3L (BNIP3-like, also known as NIX), which are 56% identical [2, 10], FUNDC1 (FUN14 domain-containing protein 1), etc. [11, 12]. In the regulation of mitophagy by these proteins, posttranslational modifications play a key role in various kinds of stimuli [13]. The regulation mechanisms of FUNDC1- and PINK1/Parkin-mediated mitophagy have been well illustrated [14, 15]. However, until now, the mechanisms underlying BNIP3/BNIP3L-mediated mitophagy, especially under hypoxic conditions, have been far from clear. It has been demonstrated that the phosphorylation of BNIP3 at Ser 17/24 and BNIP3L at Ser 34/35 or Ser 81 enhances their respective association with LC3 and facilitates activation of mitophagy [16–19]. In addition, recent studies reported that phosphorylation of Ser 212 at the C-terminal of BNIP3L, which is responsible for dimerization or subcellular localization of BNIP3, is involved in the regulation of mitophagy [20, 21].

BNIP3 is a member of the atypical BH3-only subfamily within the BCL-2 family and is localized at the mitochondrial outer membrane [22, 23]. BNIP3 is transcriptionally activated by the

¹Department of Neurobiology, Beijing Institute of Basic Medical Sciences, Beijing 100850, China. ²State Key Laboratory of Proteomics, Beijing Proteome Research Center, Beijing Institute of Radiation Medicine, Beijing 100850, China. ³Beijing Institute of Microbiology and Epidemiology, Beijing 100850, China. ⁴Chinese Institute for Brain Research, Beijing 102206, China. ⁵Co-Innovation Center of Neuroregeneration, Nantong University, Nantong 226001, China. ⁶Lanzhou University School of Information Science & Engineering, Lanzhou 730000, China. ⁷These authors contributed equally: Yun-Ling He, Jian Li. ✉email: fanmingchina@126.com; wuht@bmi.ac.cn; linglingzhu@hotmail.com; liyingwu_china@163.com

Edited by Dr. Flavie Strappazon

Received: 5 April 2022 Revised: 7 November 2022 Accepted: 8 November 2022

Published online: 17 November 2022

transcription factor HIF-1 (hypoxia-inducible factor 1) under hypoxia, which is why it is extremely sensitive to hypoxia and is generally used as a typical target gene of HIF-1 [24–26]. In addition, as far as we know, BNIP3 is more sensitive to hypoxia than any of the other BH3-only proteins on the mitochondrial outer membrane [24]. The functions of BNIP3 appear to be contradictory, involving the induction of apoptosis or mitophagy in different contexts or cell types [27–31]; however, the precise mechanisms of BNIP3 functions have not been elucidated. In recent years, many studies have focused on BNIP3-mediated mitophagy, but how BNIP3 regulates mitophagy under hypoxia remains unclear. It has been demonstrated that upregulation of BNIP3 under hypoxic conditions promotes its interaction with BCL-2/BCL-XL, which contributes to the release of Beclin-1 from BCL-2/BCL-XL binding and initiates autophagy [28, 29]. However, after induction of autophagy by upregulation of BNIP3, how damaged mitochondria are recognized to initiate mitophagy in the same context has not been clarified. Some studies have reported that BNIP3 overexpression promotes mitophagy by enhancing its interaction with the autophagosome membrane protein LC3 [32, 33]. Here, we demonstrate that BNIP3 phosphorylation, rather than its overexpression, plays a decisive role in mediating mitophagy.

In this study, we identified the new phosphorylation site Ser 60/Thr 66 in BNIP3. Most importantly, we identified JNK1/2 (c-Jun N-terminal kinase 1/2) and PP1/2A (protein phosphatase 1/2A) as the kinase and phosphatase responsible for phosphorylation and dephosphorylation, respectively, of BNIP3 at Ser 60/Thr 66 residue in response to hypoxia. Furthermore, we demonstrated that phosphorylation of BNIP3 by JNK1/2 is required for both induction of mitophagy and increased stability of BNIP3, while dephosphorylation of BNIP3 by PP1/2A causes proteasomal degradation of BNIP3 and accordingly failure of mitophagy induction. To the best of our knowledge, the mechanisms by which BNIP3 is degraded via the ubiquitin-proteasome pathway have not previously been revealed. Here, we report the crosstalk between BNIP3-mediated mitophagy and its proteasomal degradation under hypoxic conditions. Collectively, our study shows that JNK1/2 and PP1/2A oppositely regulate BNIP3 phosphorylation and consequently manipulate its stability, which in turn affects the induction of mitophagy.

MATERIALS AND METHODS

Cell culture and hypoxia treatment

PC12, HeLa and HEK293T cells were obtained from American Type Culture Collection (ATCC). Cells were cultured in RPMI-1640 Medium (HyClone, SH30027) supplemented with 1% penicillin-streptomycin (HyClone, SV30010) and 5% fetal bovine serum, 10% horse serum (Thermo Fisher Scientific) or Dulbecco's modified Eagle's medium (DMEM, HyClone, SH30081) supplemented with 1% penicillin-streptomycin and 10% fetal bovine serum at 37 °C under 5% CO₂. PC12 and HeLa cells stably expressing Flag-BNIP3 or mt-Keima were selected in media containing 1 µg ml⁻¹ puromycin (Thermo Fisher Scientific, A1113802). For hypoxia treatment, cells were placed in an incubator (Thermo Fisher Scientific) at 37 °C with 20% O₂ and 5% CO₂ for 24 h, and then moved to a hypoxia chamber (0.3% O₂, 5% CO₂ and 94.7% N₂ (Coy laboratory) or 10% O₂, 5% CO₂ and 85% N₂ (Thermo Fisher Scientific).

Reagents and antibodies

Mitotracker (M7512) was purchased from Thermo Fisher Scientific; λ-PPase (P0753) was obtained from New England Biolabs; 3-MA (M9281), cycloheximide (01810), K252c (S3939), MG132 (M7449), okadaic acid (O8010), and TBB (T0826) were from Sigma-Aldrich; Bafilomycin A1 (S1413), Bis I (S7208), JNK-IN-8 (S4901), PD184352 (S1020), Roscovitine (S1153), SB203580 (S1076), and SP600125 (S1460) were from Selleck; Calyculin A (1336) was purchased from Tocris.

The following antibodies were used for western blotting: anti-BNIP3 (1:1000, mouse mAb, Abcam, ab10433), anti-p62 (1:10,000, mouse mAb, Abcam, ab56416), anti-phospho-BNIP3 (Ser 60, 1:400, rabbit pAb) was

generated by Abclonal, anti-BCL-2 (1:1000, mouse mAb, BD bioscience, 610538), anti-JNK1 (1:1000, mouse mAb, Cell Signaling Technology, 3708), anti-JNK2 (1:1000, rabbit mAb, Cell Signaling Technology, 9258), anti-JNK3 (1:500, rabbit mAb, Cell Signaling Technology, 2305), anti-PP2A (1:1000, rabbit pAb, Cell Signaling Technology, 2038), anti-p-MAPK/CDK substrates (1:500, rabbit mAb, Cell Signaling Technology, 2325), anti-p-SAPK/JNK (1:1000, rabbit pAb, Cell Signaling Technology, 9251), anti-SAPK/JNK (1:1000, rabbit pAb, Cell Signaling Technology, 9252), anti-Flag (anti-DDDDK, 1:10,000, mouse mAb, MBL, M185-3), anti-Flag (anti-DDDDK, 1:2000, rabbit pAb, MBL, PM020), anti-HIF-1α (1:1000, mouse mAb, Novus Biologicals, NB100-105), anti-c-Myc (1:1000, rabbit pAb, Santa Cruz, sc-789), anti-GFP (1:1000, rabbit pAb, Santa Cruz, sc-8334), anti-GST (1:1000, mouse mAb, Santa Cruz, sc-1138), anti-HA (1:1000, rabbit pAb, Santa Cruz, sc-805), anti-PP1 (1:1000, mouse mAb, Santa Cruz, sc-7482), anti-TOMM20 (1:5000, rabbit pAb, Santa Cruz, sc-11415), anti-Ub (1:1000, mouse mAb, Santa Cruz, sc-8017), anti-LC3B (1:4000, rabbit pAb, Sigma-Aldrich, L7543) and anti-β-actin (1:10,000, mouse mAb, Sigma-Aldrich, A5316). The following HRP-conjugated secondary antibodies were used for western blotting: goat anti-mouse IgG (1:2000, MBL, 330) and goat anti-rabbit IgG (1:2000, MBL, 458). The following antibodies were used for immunofluorescence experiments: anti-Flag (anti-DDDDK, 1:1000, mouse mAb, MBL, M185-3), anti-Flag (anti-DDDDK, 1:1000, rabbit pAb, MBL, PM020), anti-HA (1:1000, mouse mAb, MBL, M180-3) and anti-TOMM20 (1:1000, rabbit pAb, Santa Cruz, sc-11415). The fluorescent secondary antibodies were conjugated with either Alexa Fluor 594 (1:1000, anti-rabbit, Cell Signaling Technology, 8889) or Alexa Fluor 647 (1:1000, anti-mouse, Cell Signaling Technology, 4410). Mouse IgG (C2118) was purchased from Applygene.

Plasmids, transfection, and virus production

BNIP3 was amplified from rat cDNA (NCBI RefSeq NM_053420.3) via PCR and fused with Flag via an N-terminal epitope tag. Then, Flag-tagged BNIP3 was cloned into a pcDNA3.1 vector (Thermo Fisher Scientific) or a pCDH vector (System Biosciences, CD550A-1). JNK1 (NCBI RefSeq NM_001323302.1) and JNK2 (NCBI RefSeq NM_002752.4) were amplified from human cDNA via PCR and cloned into a pXJ40-HA vector. Mitochondria-target Keima plasmids were amplified from pMT-monomeric-Keima-Red (MBL, AM-V0251HM) and cloned into a pCDH vector. Site-directed mutants and siRNA-resistant constructs were performed using kits according to standard methods (SBS Genetech). The primer information can be found in Supplementary Table S1. All the plasmids were verified by DNA sequencing. pXJ40-HA, pXJ40-Myc-Ub, pEGFP-C1-PPP1CA, pEGFP-C1-PPP1CC and pEGFP-C1-LC3B [34] were gifts from Q. Xia and T. Zhou (State Key Laboratory of Proteomics, Beijing). pSRα-HA-MKK7-JNK1 (JNK1^{CA}) and pSRα-HA-JNK1-APF (JNK1^{DN}) (Thr-Pro-Tyr replaced with Ala-Pro-Phe) [35] were gifts from J.-Y. Zhang (Beijing Institute of Basic Medical Sciences, Beijing).

Transfection of plasmids was performed using Lipofectamine 2000 reagent (Thermo Fisher Scientific) according to the manufacturer's instructions. For RNA interference, cells were transfected with negative control or with pre-designed siRNAs (Sigma-Aldrich or Ribobio) targeting the indicated genes (Supplementary Table S2) at a final concentration of 50 nM or 100 nM using X-tremeGene siRNA transfection reagent (Roche, 04476093001) according to the manufacturer's instructions. For lentivirus production, pCDH plasmids were co-transfected with psPAX2 and pMD2.G plasmids into HEK293T cells.

Transmission electron microscopy

After PC12 cells were exposed to different oxygen concentrations for 24 h, the cells were collected by digestion and centrifugation, washed with PBS, and then fixed with 3% glutaraldehyde in 0.075 M PBS (pH 7.4) at 4 °C for 2 h. After fixation, the cells were washed three times with PBS, post-fixed in 1% OsO₄ at 4 °C for 1 h, and washed in PBS for 15 min. Cell precipitates were dehydrated through a graded series of 50% to 90% ethanol, which was then replaced with 90% to 100% acetone. The cultures were soaked and then embedded in acrylic resin. Next, 60-nm ultrathin sections were collected on copper grids and stained with uranyl acetate for 10 min and lead citrate for 10 min. The samples were visualized and photographed using a HITACHI H-7650 transmission electron microscope at 80 kV.

Confocal imaging of living cells

For co-localization of autophagosomes and mitochondria experiments, cells were transfected with plasmid encoding GFP-LC3 for 48 h and then exposed to hypoxia or normoxia for an additional 24 h. Next, mitochondria were marked with 50 nM MitoTracker Red CMXRos at 37 °C under 5% CO₂

for 30 min, and then, the cells were washed with PBS. Cell images were captured with a confocal microscope (Carl Zeiss) and analyzed using ImageJ software (NIH). The co-localization of autophagosome and mitochondria was quantified by counting more than 40 cells.

For mt-Keima experiments, fluorescence of mt-Keima was captured in two channels using two sequential excitations (normal mitochondria, 440 nm, green; acidic mitochondria, 590 nm, red), mitophagy index was quantified by the ratio of 590 nm:440 nm fluorescence intensity from more than 30 different view fields.

Immunofluorescence microscopy

PC12 or HeLa cells were grown on glass coverslips. After the indicated treatment, cells were fixed with 4% paraformaldehyde (PFA) for 15 min at room temperature, washed three times with PBS, permeabilized with 0.5% Triton X-100 in PBS for 30 min and blocked with 5% goat serum for 1 h at room temperature. Cells were then incubated with primary antibodies diluted in goat serum overnight at 4 °C, followed by incubation with secondary antibodies diluted in goat serum for 1 h. All images were captured with a confocal microscope. For quantification of no or few TOMM20, more than 150 cells from 30 different fields were counted.

Real-time quantitative PCR

Total RNA was isolated from cells using Trizol[®] reagent (Thermo Fisher Scientific, 15596-026) according to the manufacturer's protocol. An aliquot of 1 µg of total mRNA was reversely transcribed at 42 °C for 1 h in a 10 µl reaction mixture containing oligo (dT) 18 primer, M-MLV reverse transcriptase and RNase inhibitor (TaKaRa, D2639A). Q-PCR was performed in triplicate with Power SYBR[®] Green (Thermo Fisher Scientific, 4367659) on a Step-one Plus system (Thermo Fisher Scientific). The primer information can be found in Supplementary Table S3.

SDS-PAGE and western blotting

Cells were lysed in ice-cold RIPA buffer (50 mM Tris-HCl (pH 7.4), 150 mM NaCl, 1% NP-40, and 0.1% SDS) containing a protease inhibitor cocktail (Roche, 11697498001). Equal amounts of protein were separated on 10–15% SDS-PAGE gels and transferred to PVDF membranes (Roche, 03010040001). The membranes were probed with the indicated primary antibodies followed by the appropriate HRP-conjugated secondary antibodies. The protein content was determined with a chemiluminescence (ECL) assay kit (Bio-Rad, 1705060).

Lambda phosphatase assay

PC12 cells were seeded in 60-mm dishes. After the indicated treatment, cells were washed with ice-cold PBS and lysed in RIPA buffer containing protease inhibitor cocktail. After centrifugation at 13,200 × g for 15 min at 4 °C, supernatant fractions containing equal amounts of protein (50 µg) were incubated with lambda phosphatase and the phosphatase buffer for 1 h at 37 °C. Samples were boiled and subjected to SDS-PAGE and western blotting.

Immunoprecipitation

After transfection with the indicated plasmids, HeLa cells were collected and lysed in 1 ml of lysis buffer (20 mM Tris-HCl, 150 mM NaCl, 1 mM Na₂-EDTA, 1 mM EGTA, 1% Triton X-100, 2.5 mM sodium pyrophosphate, 1 mM β-glycerophosphate, 1 mM Na₃VO₄, and 1 µg ml⁻¹ leupeptin, Cell Signaling Technology, 9803) containing protease inhibitor cocktail. After centrifugation at 13,200 × g for 15 min at 4 °C, equal amounts of cell lysates were preincubated with mouse IgG (Applygene, C2118) and Protein A/G agarose beads (Santa Cruz, sc-2003) for 4 h at 4 °C and then clarified by centrifugation. Supernatant fractions were immunoprecipitated with 2 µg indicated antibodies and 40 µl Protein A/G agarose beads overnight at 4 °C. After being washed five times, the immunoprecipitates were boiled in Laemmli sample buffer (Bio-Rad, 1610737) for 5 min. Samples were analyzed via SDS-PAGE and western blotting.

Degradation and ubiquitination assays

BNIP3 degradation was estimated using cycloheximide (CHX) chase assays. Cells were treated with 20 µg ml⁻¹ CHX for the indicated time, and cell lysates were subjected to SDS-PAGE and western blotting. For the ubiquitination assay, cells were lysed in RIPA buffer containing protease inhibitor cocktail and boiled for 10 min. After being clarified by centrifugation, cell lysates were precleared with mouse IgG and

immunoprecipitated with an anti-BNIP3 or anti-Flag antibody and Protein A/G agarose beads. Immunoprecipitated complexes were detected via SDS-PAGE and western blotting.

In vitro kinase assay

For protein purification, WT and S60/T66A of BNIP3 were cloned into the pGEX-4T-1 vector and fused with GST via an N-terminal epitope tag. *E. coli* strain BL21 (DE3) was transformed with the plasmids and harvested after induction with 0.8 mM IPTG for 4 h at 37 °C. Bacteria were sonicated lysed in 50 mM Tris-HCl, 200 mM NaCl, 1 mM EDTA, 1 mM DTT, and 5% glycerol. GST proteins were purified using Glutathione Resin (Thermo Fisher Scientific, 16100) and eluted with reduced glutathione.

For in vitro kinase assay, after transfection with pSRα-HA-MKK7-JNK1 (JNK1^{CA}) or pSRα-HA-JNK1-APF (JNK1^{DN}) plasmids, HeLa cells were lysed in 1 ml of lysis buffer containing protease inhibitor cocktail. After centrifugation at 13,200 × g for 15 min at 4 °C, anti-HA antibody and Protein A/G agarose beads were added to the cell lysates, followed by incubation for 4 h at 4 °C. The immunoprecipitates were washed three times with lysis buffer and twice with kinase buffer (25 mM Tris-HCl, 5 mM β-glycerophosphate, 2 mM dithiothreitol, 0.1 mM Na₃VO₄, and 10 mM MgCl₂, Cell Signaling Technology, 9802). The reactions were performed by adding 30 µl of kinase reaction mixture (kinase buffer plus 100 µM ATP, Cell Signaling Technology, 9804 and 1 µg purified GST fusion protein) at 30 °C for 30 min. The reactions were terminated by adding Laemmli sample buffer and boiling for 5 min, phosphorylation was detected via SDS-PAGE and western blotting.

Statistical analysis

The statistical data are expressed as the mean ± SEM. Statistical significant differences were assessed using Student's t-test (Fig. S4b) or one-way analysis of variance (ANOVA) followed by Tukey's multiple comparison test (Figs. 1a, b, 2d, e, g, h, 3g, 4f, 5d, g, and 6f, Figs. S1b, c, d and S2a, b, c, e) or Dunnett's multiple comparison test (Fig. 1f, Figs. S1e and S5a) or two-way ANOVA with Tukey's multiple comparison test (Figs. 1c, 2f, 3b, d, f, 4a, b, d, e, 5b, c, and 6a–e, Figs. S2d, S4d, and S5c). Differences between compared groups were considered statistically significant at *P* values <0.05. **P* < 0.05, ***P* < 0.01, and ****P* < 0.001 versus the corresponding controls are indicated. All statistical analyses were done using GraphPad Prism 8 software.

RESULTS

Phosphorylation of BNIP3 is related to mitophagy under hypoxia

We first observed mitophagy under different hypoxia conditions using an oxygen-sensitive PC12 cell line [36], and surprisingly found that mitophagy under different hypoxia conditions is vastly different. Compared with normoxia (20% O₂), 10% O₂ promoted mitophagy and 0.3% O₂ suppressed mitophagy when cells were exposed to the different oxygen levels for the same time, based on observations of the morphological characteristics of mitochondria via transmission electron microscopy (TEM) (Supplementary Fig. S1a), quantification of the ratio of acidic (excited by 590 nm light) to normal mitochondria (excited by 440 nm light) by a pH-sensitive mitochondrial matrix-localizing Keima [34, 37–39], also known as mt-Keima (Fig. 1a), TOMM20 expression (Supplementary Fig. S1b), and the co-localization of autophagosomes and mitochondria via a fluorescence confocal microscopy (Supplementary Fig. S1c). To investigate the possible causes of different mitophagy under different hypoxia conditions, we then evaluated the effects of BNIP3 on mitophagy under different hypoxia, because BNIP3 is extremely sensitive to hypoxia stimulation except as a mitophagy receptor. Notably, we found that the BNIP3 protein was detected almost at 30 kDa in the 20% O₂ and 10% O₂ groups, while most of the bands in the 0.3% O₂ group displayed faster migration (21.5–30 kDa) and more accumulation at 24 h of exposure. Comparatively, the protein level in the upper band was higher in the 10% O₂ group than that in the 0.3% O₂ group but not the total protein level. Meanwhile, we noticed that the BNIP3 protein level in the upper band was consistent with the mitophagy activity (Fig. 1b). In addition, when *Bnip3* was knocked down with siRNA, mitophagy in the 10% O₂ group was obviously

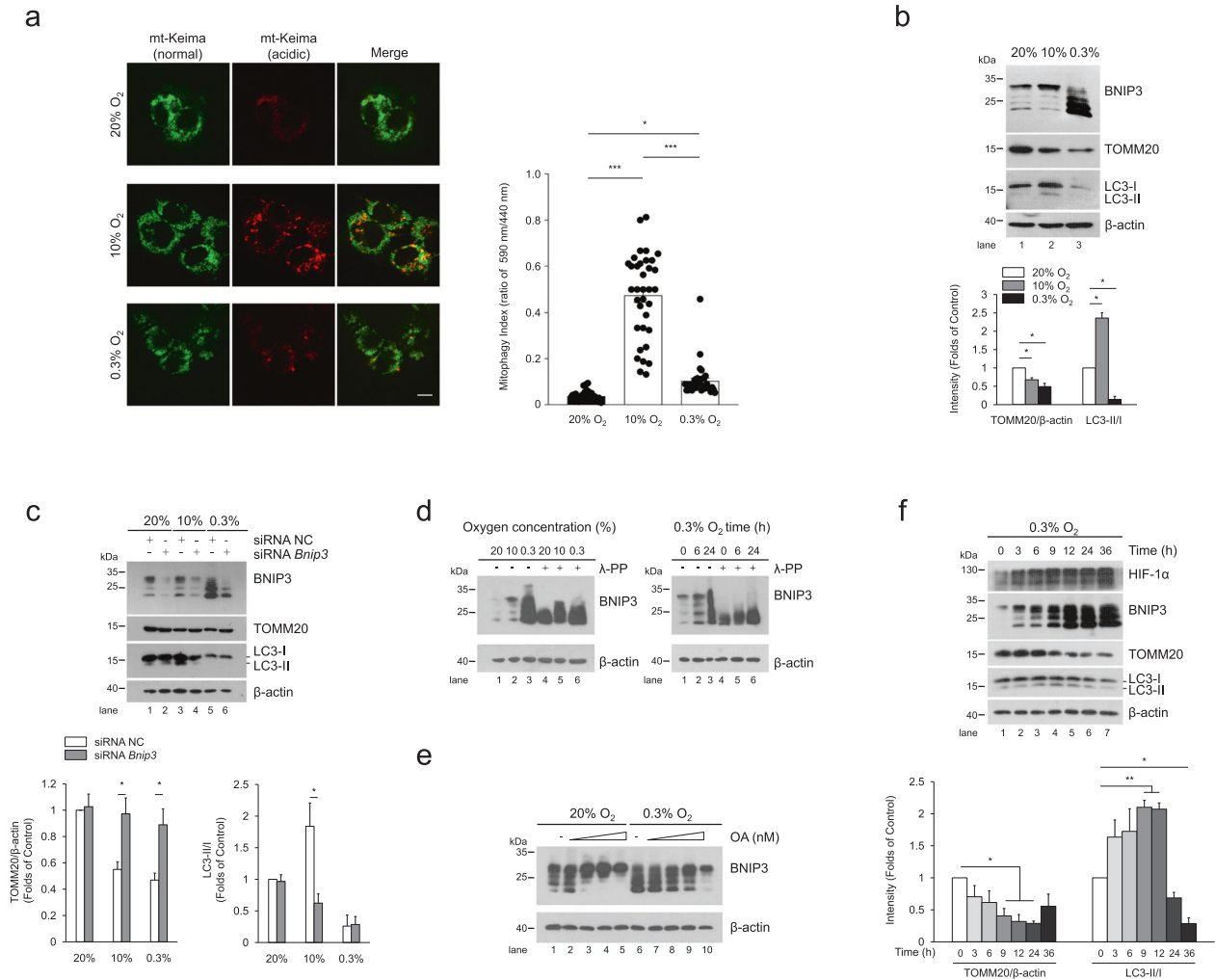


Fig. 1 **BNIP3 phosphorylation is closely related to mitophagy.** **a** PC12 cells stably expressing mt-Keima were exposed to 20% O₂, 10% O₂, or 0.3% O₂ for 24 h, and mitophagy was identified and quantified by the ratio of acidic (590 nm, red) to normal mitochondria (440 nm, green). Scale bar, 10 μm. *n* = 35. **b** PC12 cells were treated same as **(a)**, BNIP3, TOMM20 and LC3 were detected via western blotting. *n* = 3. **c** PC12 cells were transfected with negative control (NC) or *Bnip3* siRNA for 48 h and then exposed to different oxygen concentrations for 24 h. The levels of BNIP3 mitophagy-related proteins were detected via western blotting. *n* = 3. **d** PC12 cells were exposed to different oxygen concentrations for 24 h or 0.3% O₂ for the indicated times. Cell lysates were treated with/without lambda phosphatase (λ-PPase) for 1 h, followed by western blot analysis. **e** PC12 cells were exposed to 20% O₂ or 0.3% O₂ complemented with 0, 50, 100, 200, 500 nM okadaic acid (OA), and subjected to western blotting. **f** PC12 cells were exposed to 0.3% O₂ for the indicated times. Cell lysates were then western blotting for the indicated proteins. *n* = 3. The data are expressed as means ± SEM. **P* < 0.05, ***P* < 0.01, ****P* < 0.001 versus the indicated group.

attenuated, with reduced levels of the autophagosome marker LC3-II and increased levels of the mitochondrial outer membrane protein TOMM20, while knockdown of *Bnip3* in the 0.3% O₂ group did not lead to comparable differences in mitophagy (Fig. 1c). It such seems that the high BNIP3 protein level in the 0.3% O₂ group was not conducive to mitophagy activity. Taken together, these data indicate that regulation of mitophagy by BNIP3 is not completely dependent on its protein level.

Considering post-translational modifications, we speculated that phosphorylation and dephosphorylation might be involved in regulating the differences in BNIP3 protein bands. To determine if the upper band of BNIP3 was a result of phosphorylation modification, we added lambda phosphatase (λ-PPase) to cell lysates and excitedly found that all the upper bands migrated to the position around 21.5 kDa at 24 h after exposure to different oxygen concentrations or exposure for different time intervals (Fig. 1d). Conversely, after cells were exposed to the phosphatase inhibitor okadaic acid (OA), nearly all the BNIP3 protein bands gradually migrated to the position around 30 kDa as the concentration of OA was increased (Fig. 1e). From the above

results, we inferred that BNIP3 is regulated by multisite phosphorylation, and the fully phosphorylated form (hereafter referred to as phosphorylation of BNIP3) is located at 30 kDa, consistent with the description in previous reports that BNIP3 exists in multiple phosphorylated forms [40, 41]. We also observed when the levels of BNIP3 phosphorylation increased with time during early hypoxia, mitophagy was augmented, with increased LC3-II and lower TOMM20 levels; by contrast, when BNIP3 phosphorylation decreased during late hypoxia, mitophagy was suppressed, with less LC3-II and undiminished TOMM20 expression, which was verified by mt-Keima (Fig. 1f and Supplementary Fig. S1d), and similar results were obtained in the HeLa cells that is used widely for genetic engineering (Supplementary Fig. S1e). Collectively, these preliminary results demonstrate that BNIP3 phosphorylation is closely associated with mitophagy induction under hypoxia.

Phosphorylation of BNIP3 at S60/T66 is critical to promote mitophagy via enhancing its interaction with LC3

To find potential phosphorylation sites in BNIP3, we first searched the "PhosphoSite" database (<http://www.phosphosite.org>). Based

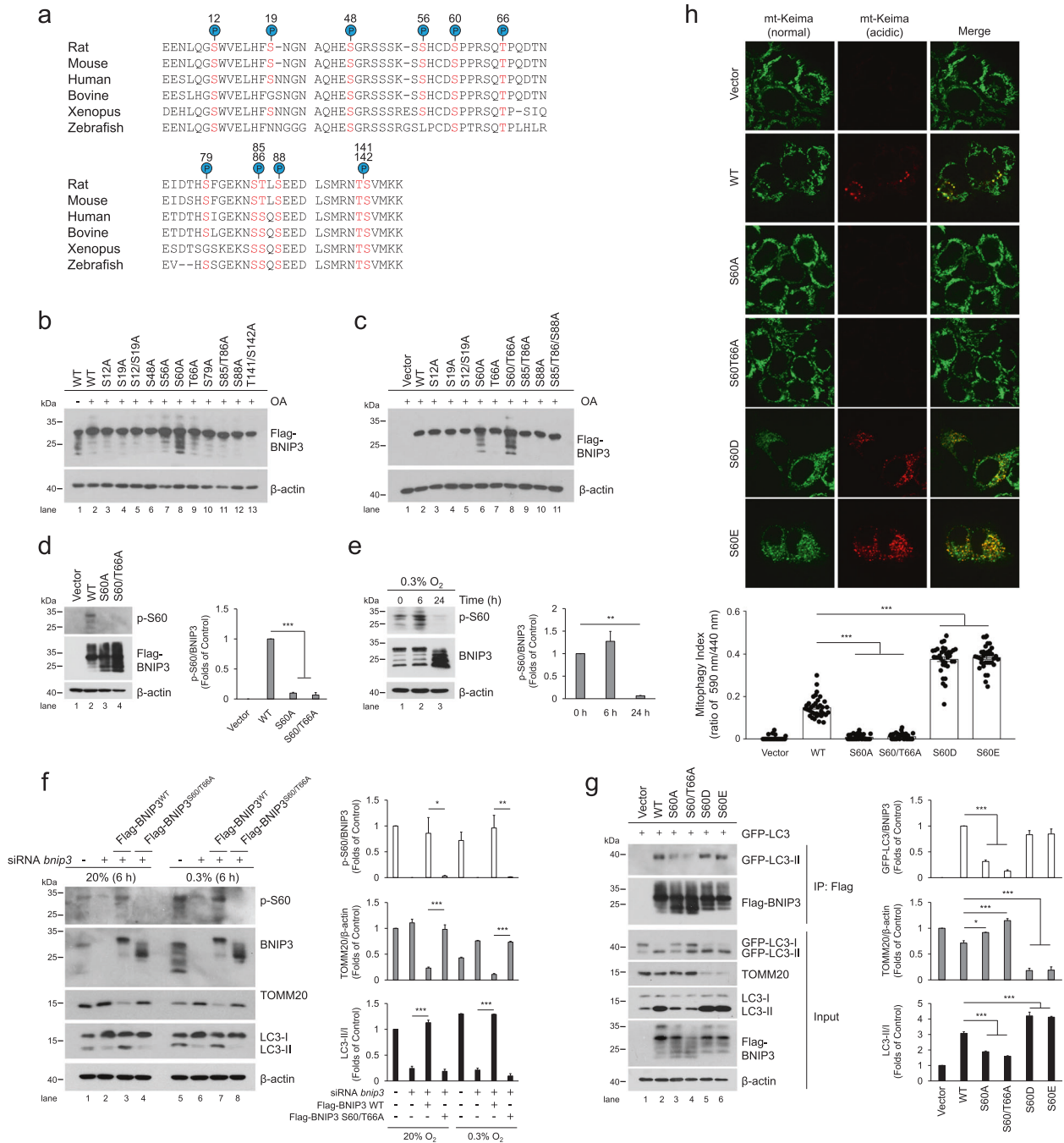


Fig. 2 Phosphorylation of BNIP3 at S60/T66 is critical to promote mitophagy by enhancing its interaction with LC3. **a** Putative BNIP3 phosphorylation sites based on reported proteomics data (PhosphoSitePlus®) that are conserved across different species. Conserved serine and threonine residues are marked in red. **b, c** HeLa cells were transfected with empty vector and Flag-BNIP3 plasmids encoding either wild-type (WT) or mutant BNIP3 constructs generated via site-directed mutagenesis. After 48 h of transfection, cell lysates were detected via western blotting with anti-Flag antibody. OA, okadaic acid. **d** HeLa cells were transfected with empty vector, WT, S60A or S60/T66A mutant Flag-BNIP3 plasmids, phosphorylation of BNIP3 was detected via western blotting using a phospho-specific antibody against BNIP3 at Ser 60 (p-S60). *n* = 3. **e** The phosphorylation level of BNIP3 at Ser 60 in PC12 cells was measured under 0.3% O₂ for the indicated time. *n* = 3. **f** PC12 cells were treated with *Bnip3* siRNA and transfected with *Bnip3* siRNA-resistant WT or S60/T66A plasmids, and then cells were exposed to 20% O₂ or 0.3% O₂ for 6 h, respectively. Mitophagy and the phosphorylation of BNIP3 were detected via western blotting. *n* = 3. **g** HeLa cells were transfected with GFP-LC3 and empty vector, WT or the indicated Flag-BNIP3 mutants for 48 h. Cell lysates were immunoprecipitated with anti-Flag antibody and then subjected to western blot analysis with the indicated protein antibodies. *n* = 3. **h** The indicated plasmids were transfected into HeLa cells stably expressing mt-Keima and cell images were captured with a confocal microscope. Mitophagy was identified and quantified by the ratio of acidic (590 nm, red) to normal mitochondria (440 nm, green). Scale bar, 10 μm. *n* = 35. The data are expressed as means ± SEM. **P* < 0.05, ***P* < 0.01, ****P* < 0.001 versus the indicated group.

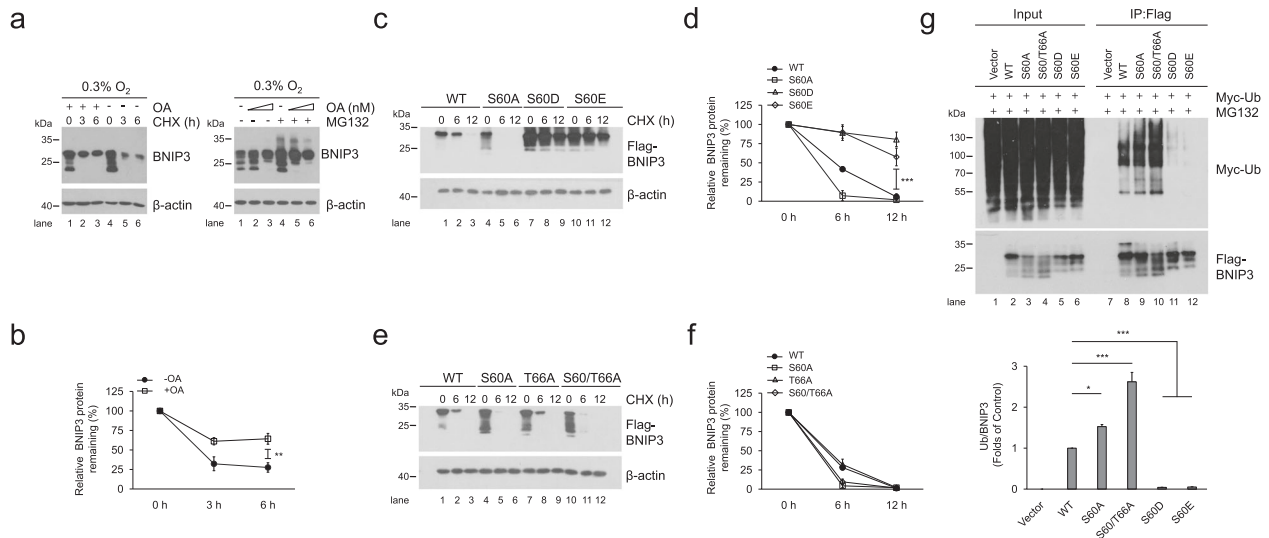


Fig. 3 Phosphorylation of BNIP3 at S60/T66 is essential to improve its stability. **a** PC12 cells were exposed to 0.3% O₂ supplemented with 200 nM okadaic acid (OA) for 12 h and then treated with 20 μg ml⁻¹ cycloheximide (CHX) for the indicated times (left panel) or with 100, 200 nM OA plus 10 μM MG132 for 6 h (right panel). Cell lysates were detected via western blotting using the indicated antibodies. **b** Quantification of degradation rate of BNIP3 in CHX chase experiments shown in (a). **c–f** HeLa cells were transfected with plasmids encoding WT or the indicated BNIP3 mutants for 48 h and then treated with 20 μg ml⁻¹ CHX for 0 h, 6 h, or 12 h. BNIP3 expression was detected via western blotting. **d** and **f** are quantification of degradation rate of BNIP3 shown in (c) and (e), respectively. **g** HeLa cells were transfected with Myc-Ub and empty vector, WT or the indicated BNIP3 mutant for 48 h and treated with 10 μM MG132 for 12 h. Cell lysates were boiled and immunoprecipitated with an anti-Flag antibody. The immune complexes were then analyzed via western blotting. *n* = 3. The data are expressed as means ± SEM. **P* < 0.05, ***P* < 0.01, ****P* < 0.001 versus the indicated group.

on reported proteomics data, a total of 12 BNIP3 phosphorylation events based on mass spectra evidence are shown in the schematic in Fig. 2a, which represent highly conserved serine or threonine (S/T) residues across vertebrates. To further determine the specific phosphorylation sites that affect the migration of BNIP3 protein bands, mutants were constructed in which each of the 12S/T residues was changed to alanine (A) via site-directed mutagenesis to inactivate phosphorylation. HeLa cells were transfected with Flag-tagged BNIP3-S/T to A mutants, and the protein phosphorylation was assessed on the basis of changes in the migration of the protein bands after treatment with OA. The results revealed that S/T-to-A replacement at Ser 60 (S60A) blocked the upshift of BNIP3 protein bands (Fig. 2b) and double replacement at Ser 60 and Thr 66 (S60/T66A) potentiated this effect (Fig. 2c), given that these two sites have the common motif recognized by MAPKs (mitogen-activated protein kinases) or CDKs (cyclin-dependent kinases). These data indicate that Ser 60 and Thr 66 are the potential phosphorylation sites of BNIP3 and the former is the primary one, the latter is synergistic. To validate the two phosphorylation sites of BNIP3, we first immunoprecipitated Flag-BNIP3 and tested the precipitates with an antibody against phospho-MAPK/CDK substrates. As expected, both the S60A and S60/T66A mutants reduced the levels of potential phosphorylation of BNIP3 compared to wild-type (WT) (Supplementary Fig. S2a). Then, we produced a specific antibody directed to phospho-Ser 60 (p-S60) of BNIP3. This antibody recognized WT, but not the S60A and S60/T66A mutants (Fig. 2d). Using the p-S60 antibody we observed that BNIP3 phosphorylation was increased slightly in the early stage of hypoxia and reduced in the late stage of hypoxia (Fig. 2e). Altogether, these data suggest that Ser 60 is the primary phosphorylation site of BNIP3. Thereafter, we also examined the effects of hypoxia on phosphorylation of BNIP3 at Ser 60 and the effects of disabling phosphorylation at Ser 60/Thr 66 on mitophagy in one experiment. It is clear that hypoxia increased the phosphorylation of BNIP3 at Ser 60 and promoted mitophagy with reduced TOMM20 and increased LC3-II. Introduction of siRNA-resistant phosphorylation-disabled S60/T66A mutant after *Bnip3* knockdown with siRNA impaired the effect

of hypoxia on mitophagy (Fig. 2f). These results indicate that the phosphorylation of BNIP3 at Ser 60/Thr 66 is required for promoting mitophagy.

According to previous studies that upregulation of BNIP3 in hypoxia competes with Beclin-1 to interact with BCL-2, followed by release of Beclin-1 and induction of mitophagy [28, 29], we next investigated whether the phosphorylation of BNIP3 at Ser 60/Thr 66 site could affect its association with BCL-2 and thus affect the induction of mitophagy. Regrettably, all mutations of BNIP3 displayed no significant differences in interaction with BCL-2 compared to the WT BNIP3 (Supplementary Fig. S2b), suggesting that the phosphorylation of BNIP3 at least at Ser 60/Thr 66 site is not related with the interaction between BNIP3 and BCL-2. After that, we examined whether the phosphorylation of BNIP3 Ser 60/Thr 66 would affect its binding to LC3. Cells expressing GFP-tagged LC3 and Flag-tagged WT or mutant BNIP3 were collected for co-IP assays. In line with previous studies [32, 33], GFP-LC3-II was co-precipitated with BNIP3 WT, whereas the interaction was abated by S60A or S60/T66A mutant and mitophagy was inhibited. On the other hand, a BNIP3-S60 to aspartic acid (S60D) or to glutamic acid (S60E) mutation that mimics phosphorylation could maintain the binding affinity between BNIP3 and GFP-LC3-II and increased mitophagy (Fig. 2g and Supplementary Fig. S2c). To demonstrate further whether the phosphorylation of BNIP3 at Ser 60/Thr 66 impacts mitophagy, we used bafilomycin A1 (Baf A1) to block autophagy and found that LC3 and TOMM20 accumulated less in the S60A and S60/T66A groups than in the BNIP3 WT group after Baf A1 treatment (Supplementary Fig. S2d). Moreover, we expressed these BNIP3 mutants in cells and detected mitophagy via fluorescence confocal microscopy. We confirmed that the S60A and S60/T66A mutants inhibited mitophagy, while the S60D and S60E mutants induced more pronounced mitophagy, as shown by the appearance of more acidic mt-Keima (Fig. 2h) or more LC3 puncta with fewer mitochondria (Supplementary Fig. S2e). Taken together, these results indicate that phosphorylation of BNIP3 at Ser 60/Thr 66 is critical for its interaction with LC3 and induction of mitophagy.

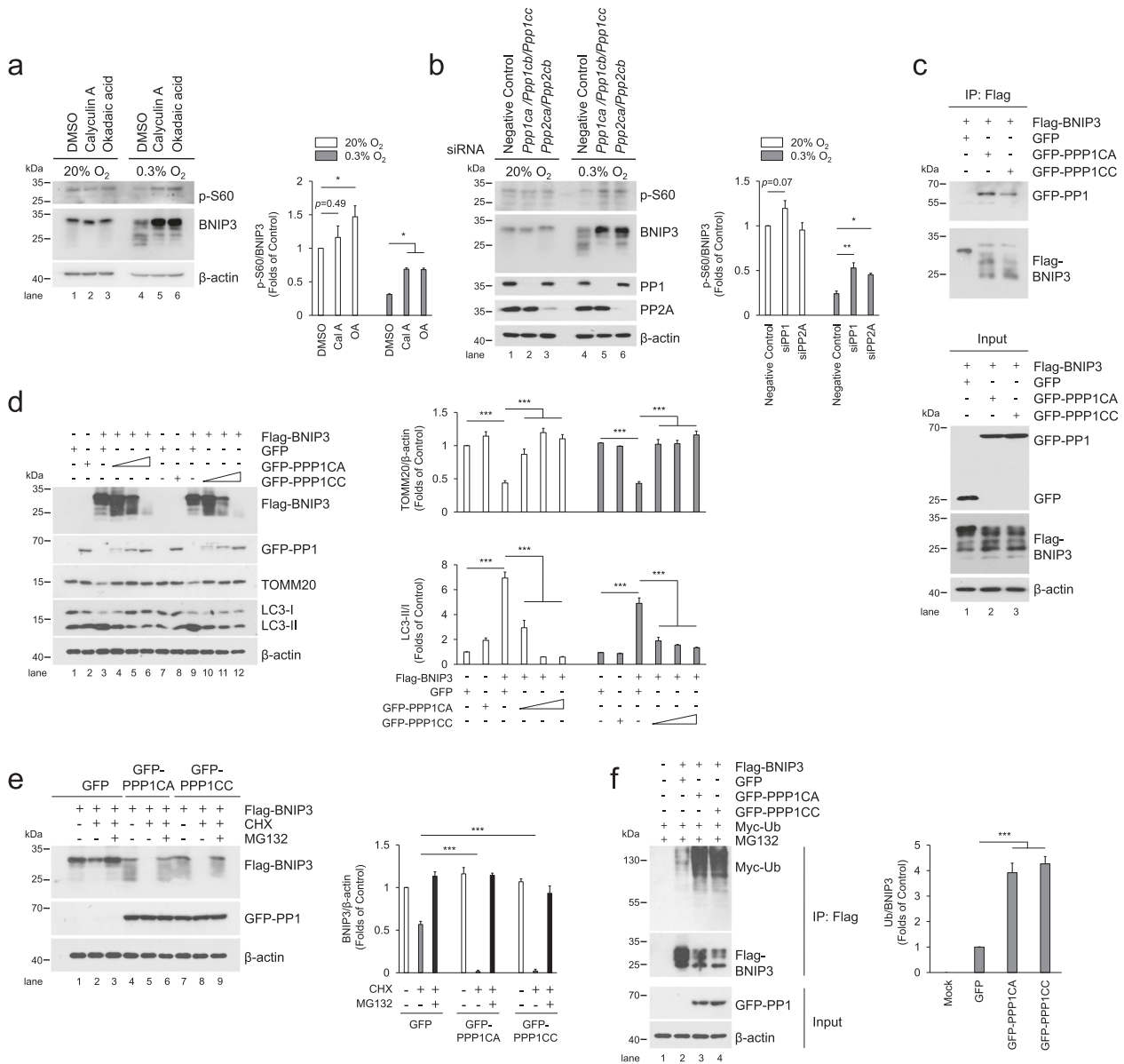


Fig. 4 PP1 and PP2A are phosphatases for BNIP3 and suppresses mitophagy by accelerating BNIP3 proteasomal degradation. **a** PC12 cells were treated with PP1 and PP2A inhibitors, Calyculin A (Cal A, 5 nM) and okadaic acid (OA, 200 nM) and then exposed to 20% O₂ or 0.3% O₂ for 24 h, the phosphorylation of BNIP3 was detected via western blotting. $n = 3$. **b** PP1 and PP2A were knocked down with siRNA targeting their respective catalytic subunits, *Ppp1ca*, *Ppp1cb*, *Ppp1cc*, and *Ppp2ca*, *Ppp2cb*, and then exposed to 20% O₂ or 0.3% O₂ for 24 h, after that, western blotting was used to detect the phosphorylation of BNIP3. $n = 3$. **c** HeLa cells were co-transfected with GFP-Vector, GFP-PPP1CA or GFP-PPP1CC and Flag-BNIP3 for 48 h, and cell lysates were then immunoprecipitated with an anti-Flag antibody and subjected to western blotting with an anti-GFP or anti-Flag antibody. **d** HeLa cells were transfected with Flag-BNIP3 and GFP-Vector or increasing concentrations of GFP-PPP1CA/PPP1CC plasmids (0.25, 0.5, 1.25 $\mu\text{g ml}^{-1}$) for 48 h, and cell lysates were then analyzed by western blotting with the indicated antibodies. $n = 3$. **e** HeLa cells were co-transfected with Flag-BNIP3 and GFP-Vector, GFP-PPP1CA or GFP-PPP1CC. At 48 h after transfection, the cells were treated with or without 20 $\mu\text{g ml}^{-1}$ CHX or 10 μM MG132 for 12 h. The degradation of BNIP3 was assessed by western blotting with the indicated antibodies. $n = 3$. **f** HeLa cells were co-transfected with Flag-BNIP3, Myc-Ub and GFP-Vector or GFP-PPP1CA/GFP-PPP1CC for 48 h, and 10 μM MG132 was added 12 h prior to sample collection. Cell lysates were boiled and immunoprecipitated with an anti-Flag antibody. The immune complexes were then analyzed via western blotting. $n = 3$. The data are expressed as means \pm SEM. * $P < 0.05$, ** $P < 0.01$, *** $P < 0.001$ versus the indicated group.

Phosphorylation of BNIP3 at S60/T66 is essential to improve its stability

In addition to the correlation with mitophagy, BNIP3 phosphorylation is also related to its stability. It has been reported that BNIP3 contains the PEST domain and can be degraded by ubiquitin-proteasome pathway [42]. Both Ser 60 and Thr 66 are located in the PEST domain, implying that BNIP3 phosphorylation may be involved in regulating its stability. We further

demonstrated that BNIP3 directly interacted with ubiquitin via ubiquitination assays (Supplementary Fig. S3). In addition, we unexpectedly found that the phosphatase inhibitor OA hindered rapid degradation of BNIP3 when protein synthesis was inhibited with cycloheximide (CHX) under 0.3% O₂ conditions. The proteasome inhibitor MG132 led to more protein accumulated, but as the concentration of OA increased, the accumulation of BNIP3 by MG132 was reduced (Fig. 3a, b), indicating that

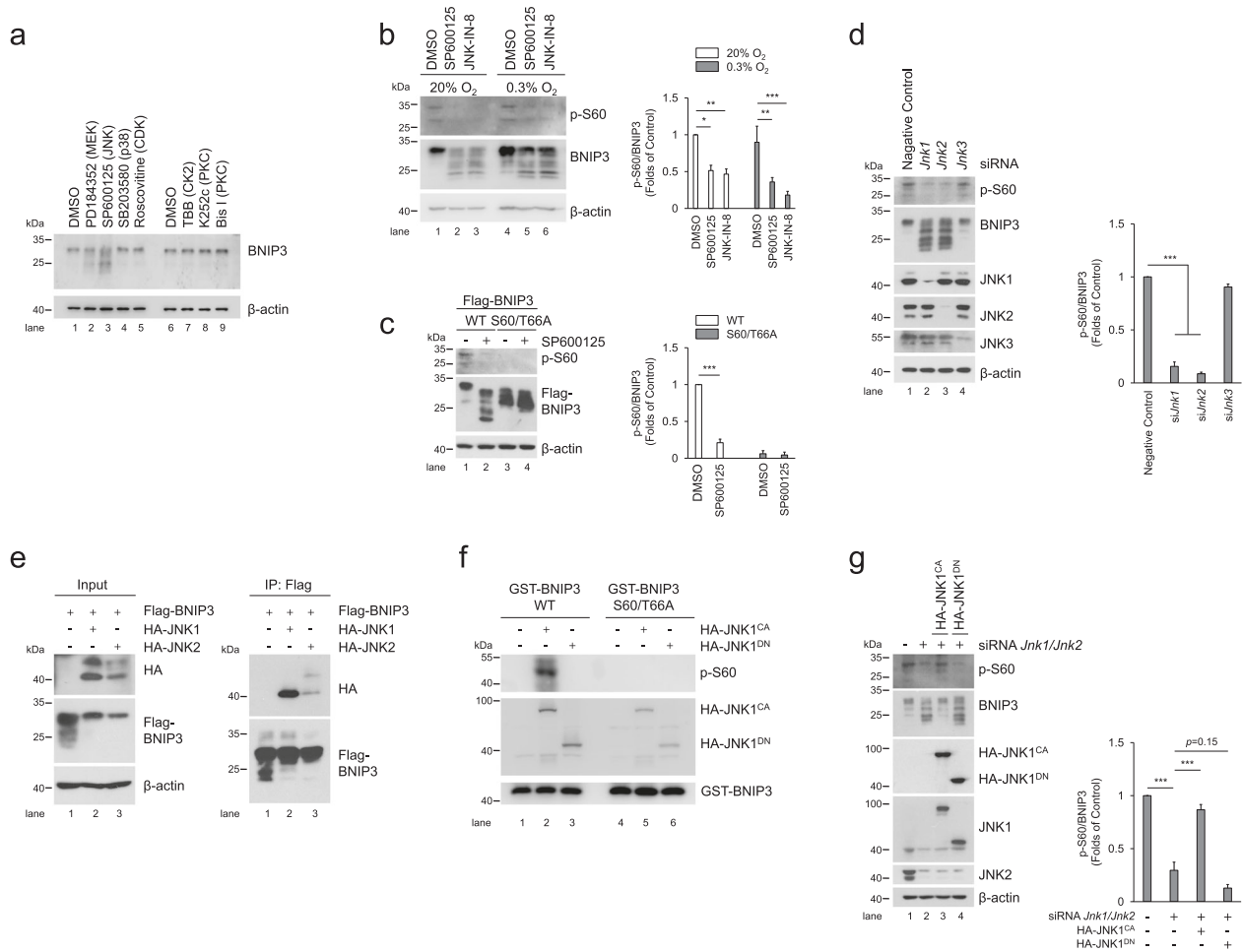


Fig. 5 JNK1/2 is the kinase responsible for BNIP3 phosphorylation. **a** PC12 cells were treated with various kinase inhibitors, including 10 μ M PD184352 (MEK inhibitor), 10 μ M SP600125 (JNK inhibitor), 10 μ M SB203580 (p38 inhibitor), 10 μ M Roscovitine (CDK inhibitor), 100 μ M TBB (CK2 inhibitor), 10 μ M K252c and 1 μ M Bis I (PKC inhibitor). Then, cell lysates were subjected to western blotting with the indicated antibodies. DMSO, dimethylsulfoxide. **b** The phosphorylation of BNIP3 was detected via western blotting after PC12 cells were treated with JNK inhibitor SP600125 (10 μ M) or JNK-IN-8 (10 μ M) and exposed to 20% O₂ or 0.3% O₂ for 6 h. $n = 3$. **c** PC12 cells stably expressing WT or S60/T66A mutant Flag-BNIP3 were treated with DMSO or SP600125 and followed by detection of phosphorylation of BNIP3. $n = 3$. **d** After *Jnk* was knocked down with the indicated siRNA in PC12 cells, the levels of JNK protein and BNIP3 phosphorylation were measured by western blotting. $n = 3$. **e** HeLa cells were transfected with Flag-BNIP3 and HA-JNK1 or HA-JNK2 for 48 h. Cell lysates were then immunoprecipitated with an anti-Flag antibody and detected by western blotting with an anti-HA or anti-Flag antibody. **f** Immunoprecipitated constitutively active (CA) HA-JNK1 or dominant negative (DN) HA-JNK1 was incubated with WT or S60/T66A GST-BNIP3 protein at 30 °C for 30 min, and then the reaction products were subjected to western blotting with the indicated antibodies. **g** *Jnk1* and *Jnk2* knockdown PC12 cells were transfected with HA-JNK1^{CA} or HA-JNK1^{DN} mutants for 48 h, cell lysates were then analyzed via western blotting with the indicated antibodies. $n = 3$. The data are expressed as means \pm SEM. * $P < 0.05$, ** $P < 0.01$, *** $P < 0.001$ versus the indicated group.

BNIP3 phosphorylation may impede its proteasomal degradation. To determine whether phosphorylation at the Ser 60/Thr 66 site is involved in regulation of BNIP3 stability, we measured the effect of the phospho-disabling or phospho-mimic mutations of these sites on BNIP3 degradation after HeLa cells were transfected with the mutants and treated with CHX. Our data demonstrated that the S60A and S60/T66A mutants accelerated the degradation of BNIP3, and the S60D and S60E mutants dramatically hampered this process, suggesting that phosphorylation at Ser 60/Thr 66 is required for BNIP3 stability (Fig. 3c–f). Since ubiquitination usually leads to proteasomal degradation, we further detected the relationship between phosphorylation and ubiquitination of BNIP3. As shown in Fig. 3g, the phospho-disabling and phospho-mimic BNIP3 mutants were linked with more or fewer ubiquitin molecules than the wild-type protein, respectively, which confirmed our above findings. Collectively, these results indicate that phosphorylation of BNIP3 at Ser 60/Thr 66 promotes its stability. Thus, we propose that the

improved BNIP3 stability may be the premise and foundation for the induction of mitophagy.

Dephosphorylation of BNIP3 by PP1/2A suppresses mitophagy by facilitating BNIP3 proteasomal degradation

Since dephosphorylation of BNIP3 is negatively correlated with mitophagy (Figs. 1f and 2f), we next wondered which protein phosphatase is responsible for dephosphorylation of BNIP3. Given that OA reversed the downward shift of the BNIP3 protein bands (Fig. 1e), which indicates that OA blocks dephosphorylation of BNIP3, and more importantly, OA is a potent inhibitor of the protein phosphatases PP1 and PP2A [43], we therefore speculate that PP1 and PP2A may be the phosphatases of BNIP3. Comparing calcyculin A (Cal A) and OA, which are more potent inhibitors of PP1 and PP2A, respectively, we observed both Cal A and OA are all effective in preventing BNIP3 dephosphorylation (Fig. 4a). To determine which catalytic subunit of PP1 or PP2A to play the key role in regulation of BNIP3 dephosphorylation, we found when all

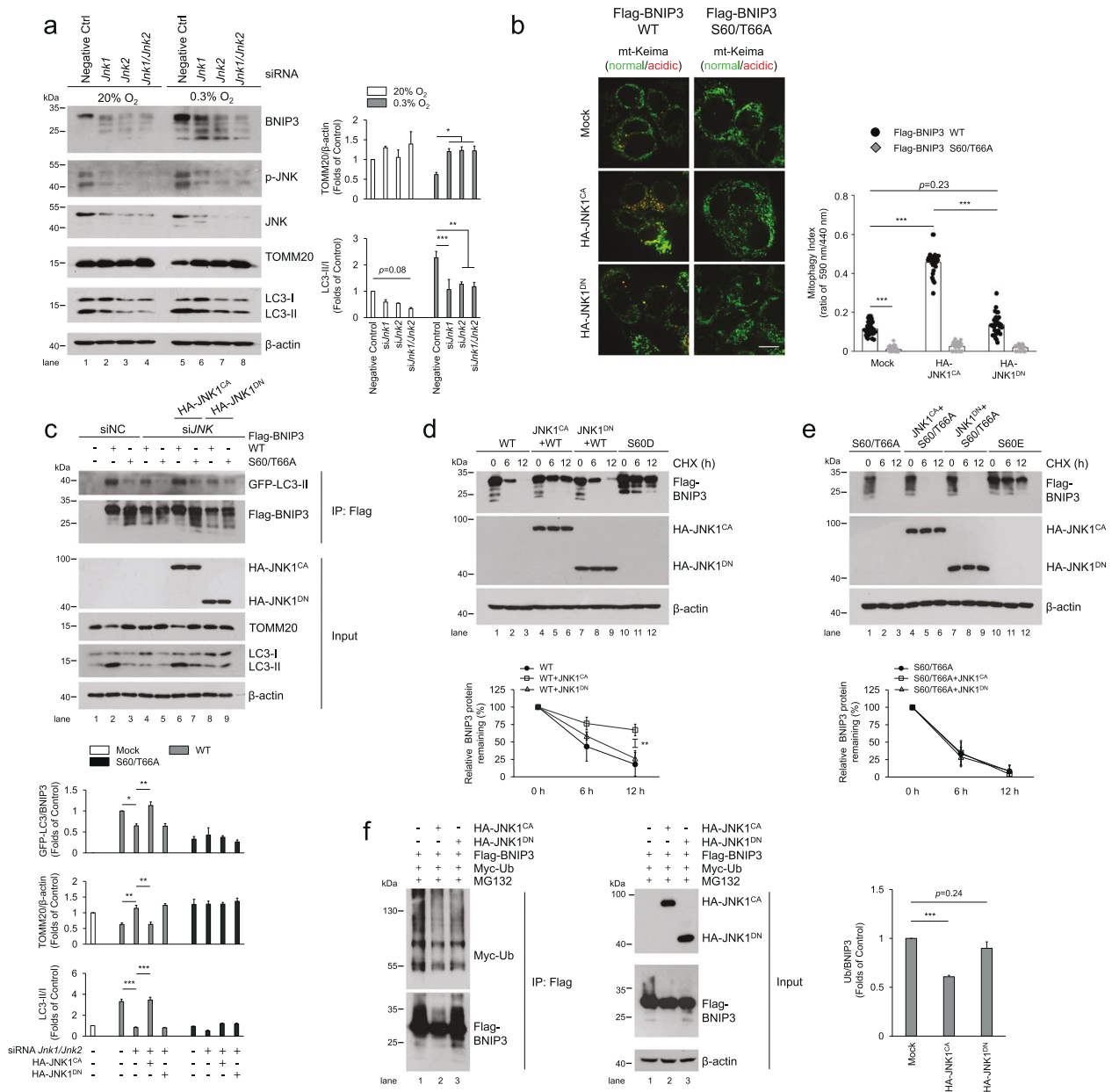


Fig. 6 Phosphorylation of BNIP3 at S60/T66 by JNK enhances mitophagy and impedes BNIP3 proteasomal degradation. **a** PC12 cells were transfected with negative control (NC), *Jnk1* and *Jnk2* siRNA for 48 h and then exposed to 20% O₂ or 0.3% O₂ for 6 h, and cell lysates were subjected to western blot analysis with the indicated antibodies. *n* = 3. **b** HeLa Cells stably expressing mt-Keima were co-transfected with plasmids encoding constitutively active (CA) or dominant negative (DN) HA-JNK1 and Flag-BNIP3 WT or S60/T66A, and mitophagy was identified and quantified by the ratio of acidic (590 nm, red) to normal mitochondria (440 nm, green). Scale bar, 10 μm. *n* ≥ 30. **c** HeLa cells were transfected with NC or *JNK1* and *JNK2* siRNA and plasmids encoding GFP-LC3. After 48 h, the cells were transfected with plasmids encoding wild-type (WT) or S60/66 A Flag-BNIP3 and HA-JNK1^{CA} or HA-JNK1^{DN} for an additional 24 h. Cell lysates were immunoprecipitated with an anti-Flag antibody and examined via western blotting with the indicated antibodies. *n* = 3. **d, e** HeLa cells were co-transfected with constitutively active or dominant negative HA-JNK1 and BNIP3 WT (**d**, left) or the S60/T66A mutants (**e**, right). After transfection for 48 h, 20 μg ml⁻¹ CHX was added to the cultures for the indicated time, and the degradation of BNIP3 was detected via western blotting with the indicated antibodies and quantified, respectively. **f** HeLa cells were co-transfected with Flag-BNIP3, Myc-Ub and constitutively active or dominant negative HA-JNK1 for 48 h, and 10 μM MG132 was added 12 h before samples were collected. Cell lysates were boiled and immunoprecipitated with an anti-Flag antibody. The immune complexes were then analyzed via western blotting. *n* = 3. The data are expressed as means ± SEM. **P* < 0.05, ***P* < 0.01, ****P* < 0.001 versus the indicated group.

catalytic subunits of PP1 or PP2A were knocked down at the same time, the effect of PP1 or PP2A knockdown was manifested, in other words, inhibition of PP1 or PP2A expression increased the level of BNIP3 phosphorylation after cells were exposed to hypoxia instead of normoxia (Fig. 4b). In addition, we also noticed that the role of PP1 is slightly stronger than PP2A. Therefore, we focused on determining whether PP1 interacts with BNIP3 and affects

BNIP3-mediated mitophagy. We co-transfected HeLa cells with PPP1CA or PPP1CC (two main catalytic subunits of PP1) combined with BNIP3 plasmids and observed the effect of PPP1CA/C on BNIP3 phosphorylation and the interaction between them using a co-IP assay. As expected, PPP1CA/C caused remarkable dephosphorylation of BNIP3 when PPP1CA/C was overexpressed in cells. In the meantime, when BNIP3 was immunoprecipitated with a

Flag antibody, PPP1CA/C was also pulled down, demonstrating an interaction between PP1 and BNIP3 in cells (Fig. 4c). To examine the effect of PP1 on BNIP3-mediated mitophagy, we co-transfected cells with BNIP3 and PPP1CA/C. Then, we found that with increasing amounts of PPP1CA/C plasmids, mitophagy was inhibited synchronously (Fig. 4d). These data indicate that PPP1CA/C is a phosphatase that dephosphorylates BNIP3, which largely results in suppression of mitophagy.

As to how PP1/2A obstructs mitophagy, considering that phosphorylation of BNIP3 improved its stability and promoted mitophagy, we speculated that dephosphorylation of BNIP3 by PP1/2A might negatively regulate the stability of BNIP3, thus leading to failure of mitophagy induction. In addition, we have noticed that the highest concentration of PPP1CA/C leads to nearly complete disappearance of BNIP3, as shown in Fig. 4d, which greatly suggests a negative regulatory effect of PP1 on the stability of BNIP3. Accordingly, we tested the effect of PP1 on the stability of BNIP3 after cells were co-transfected with PPP1CA/C and BNIP3 and then treated with CHX or MG132. We observed an increase in BNIP3 degradation induced by CHX treatment in the pEGFP-C1 control, and the degradation of BNIP3 was exacerbated by PPP1CA/C but blocked by MG132 (Fig. 4e), suggesting that PP1 accelerates BNIP3 degradation via the proteasome pathway. We further demonstrated that PP1 facilitated conjugation of BNIP3 with ubiquitin when cells were co-transfected with PPP1CA or PPP1CC and BNIP3 and Ub plasmids (Fig. 4f), suggesting that PP1 potentiates the degradation of BNIP3 via the ubiquitin-proteasome pathway. Collectively, our results demonstrate that PP1/2A is a phosphatase of BNIP3 and suppresses BNIP3-mediated mitophagy, primarily due to accelerated BNIP3 degradation via the ubiquitin-proteasome pathway.

JNK1/2 is the kinase responsible for phosphorylation of BNIP3 at S60/T66

Subsequently, we sought to identify which kinases are responsible for the phosphorylation of BNIP3 Ser 60/Thr 66 to better understand the mechanism by which BNIP3 is phosphorylated and thereby mediates mitophagy activation. Since the Ser 60/Thr 66 residue within the consensus motif of MAPKs and CDKs, we screened BNIP3-specific kinases using the respective inhibitors of MAPKs and CDKs. The results showed that the JNK inhibitor SP600125 and MEK1/2 (mitogen-activated protein kinase kinase 1/2) inhibitor PD184352 caused a marked decrease in BNIP3 phosphorylation and an increase in the dephosphorylated forms of BNIP3. Cell cycle-related inhibitors, such as Roscovitine (a selective CDK inhibitor), did not significantly affect the features of BNIP3 protein bands, suggesting that BNIP3 is not a phosphorylation substrate of CDKs. Another MAPK inhibitor, SB203580 (a specific p38-MAPK inhibitor), did not have an apparent impact on the BNIP3 protein bands. In addition, neither K252c nor Bis I (selective PKC inhibitors) nor TBB (a selective CK2 inhibitor) affected the features of BNIP3 protein bands (Fig. 5a), although PKC and CK2 have ever been reported to be related to phosphorylation of BNIP3 or other mitophagy receptors [16, 40, 44, 45]. We then combined SP600125 or PD184352 and OA to treat cells and observed that the upshift of BNIP3 protein bands caused by OA was partly reversed by SP600125 but not affected by PD184352 (Supplementary Fig. S4a). Moreover, two different JNK inhibitors, SP600125 and JNK-IN-8, could reduce BNIP3 phosphorylation under normoxia or hypoxia (Fig. 5b). The above results suggest that JNK may be the potential kinase for BNIP3. We further determined the effect of SP600125 on the phosphorylation of BNIP3 at Ser 60/Thr 66 in cells expressing WT or S60/T66A mutant. Consistent with changes of BNIP3 bands, the phosphorylation of WT but not S60/T66A mutant BNIP3 was affected by SP600125 (Fig. 5c), suggesting that the Ser 60/Thr 66 residue in BNIP3 may be the target site for JNK recognition.

Given that SP600125 is a broad-spectrum JNK inhibitor for JNK1, JNK2, and JNK3 and PD184352 inhibits ERK1/2 and ERK5 activities, we knocked them down with their respective siRNA to identify the specific BNIP3 kinases. When *Jnk1*, *Jnk2*, *Jnk3*, *Erk1*, *Erk2*, or *Erk5* was separately knocked down with the corresponding siRNA, only *Jnk1* and *Jnk2* knockdown resulted in a significant downshift of BNIP3 bands (Supplementary Fig. S4b), which illustrates that JNK1 and JNK2 are the potential kinases for BNIP3 phosphorylation. Subsequently, we confirmed that JNK1 and JNK2, but not JNK3, are the kinases of BNIP3, since knockdown of *Jnk1*, *Jnk2* but not *Jnk3* directly resulted in a decrease in BNIP3 phosphorylation levels (Fig. 5d). To investigate whether JNK1 and JNK2 interact with BNIP3 in cells, we carried out a co-IP assay after cells were co-transfected with Flag-BNIP3 and HA-JNK1 or HA-JNK2. The results showed that JNK1 had a stronger binding affinity with BNIP3 than JNK2 (Fig. 5e). Hence, we used constitutively active (CA) or dominant negative (DN) JNK1 to further test the interaction of JNK1 with BNIP3. As expected, BNIP3 interacted with CA-JNK1 but not DN-JNK1 (Supplementary Fig. S4c), demonstrating that the kinase activity of JNK1 is required for the interaction with BNIP3. To elucidate whether Ser 60/Thr 66 of BNIP3 is the phosphorylation site for JNK1, we knocked down *JNK1* and *JNK2* and then overexpressed CA-JNK1 or DN-JNK1 to examine their effects on the phosphorylation of BNIP3 WT or the S60/T66A mutant. The results showed that CA-JNK1 phosphorylated BNIP3 WT instead of the S60/T66A mutant and that DN-JNK1 had no significant effects on phosphorylation (Supplementary Fig. S4d), suggesting that Ser 60/Thr 66 of BNIP3 is the phosphorylation site for JNK1. Further, in vitro kinase assays showed that CA-JNK1 but not DN-JNK1 was able to phosphorylate BNIP3 (Fig. 5f). Consistent with this, the effect of JNK1 activity on phosphorylation of BNIP3 was verified by using a phospho-specific antibody (Fig. 5g). Taken together, these data demonstrate that JNK1/2 is a pivotal kinase that phosphorylates BNIP3.

Phosphorylation of BNIP3 S60/T66 by JNK1/2 enhances mitophagy via impeding BNIP3 proteasomal degradation

To investigate the role of JNK1/2-mediated BNIP3 phosphorylation, we first observed the dynamic changes of JNK activity, BNIP3 phosphorylation, and also PP1/2A expression under hypoxia. The results showed that JNK was transiently activated by hypoxia and inactivated after 12 h of hypoxia exposure; correspondingly, BNIP3 was phosphorylated and dephosphorylated successively; while PP1 and PP2A protein levels did not change obviously during this period (Supplementary Fig. S5a). Further, we examined the effects of *Jnk1* and *Jnk2* knockdown on BNIP3 phosphorylation and mitophagy. Western blot analysis revealed that knockdown of *Jnk1* and *Jnk2* under both normoxic and hypoxic conditions obviously reduced BNIP3 phosphorylation and simultaneously inhibited mitophagy (Fig. 6a). To further clarify whether phosphorylation of BNIP3 at Ser 60/Thr 66 by JNK1/2 is involved in the regulation of mitophagy, we compared the roles of BNIP3 WT and the S60/T66A mutant in the induction of mitophagy when CA-JNK1 or DN-JNK1 was ectopically overexpressed. Fluorescence images showed that overexpression of CA-JNK1 stimulated the formation of GFP-LC3 puncta and reduced the number of mitochondria in BNIP3 WT cells but not in S60/T66A-expressing cells. Similarly, the overexpression of CA-JNK1 promoted mitophagy activity in BNIP3 WT cells but not in S60/T66A-expressing cells, while overexpression of DN-JNK1 was ineffective for the induction of mitophagy (Fig. 6b and Supplementary Fig. S5b, c). Furthermore, a rescue experiment demonstrated that CA-JNK1 instead of DN-JNK1 restored the BNIP3-LC3 interaction attenuated by *JNK1* and *JNK2* knockdown in WT but not in the S60/T66A mutant cells (Fig. 6c). Taken together, these results consistently demonstrate that JNK1/2 promotes mitophagy by phosphorylating BNIP3 at Ser 60/Thr 66.

In addition to enhancement of the interaction between BNIP3 and LC3 by JNK1/2, we also wondered whether JNK1/2 is directly

involved in regulation of BNIP3 stability via phosphorylation of the Ser 60/Thr 66 residue, since the phosphorylation of BNIP3 Ser 60/Thr 66 was shown to improve its stability. Therefore, to determine whether JNK1/2 regulates BNIP3 stability via the Ser 60/Thr 66 site, we examined the effects of JNK1 activity on the stability of BNIP3 after cells were co-transfected with the CA-JNK1 or DN-JNK1 and BNIP3 WT or mutant expression plasmids and then CHX was added to inhibit new protein synthesis. The results clearly showed that compared with BNIP3 WT without JNK1 stimulation, CA-JNK1 increased the stability of BNIP3, similar to that of S60D or S60E, while DN-JNK1 did not affect the stability of BNIP3 WT. On the other hand, neither CA-JNK1 nor DN-JNK1 altered the effect of the phosphorylation-disabled S60/T66A mutant on BNIP3 stability (Fig. 6d, e), indicating that JNK1/2 regulation of BNIP3 stability is achieved by phosphorylation of the Ser 60/Thr 66 residue. To further determine whether JNK1/2 regulation of BNIP3 stability involves the ubiquitin-proteasome pathway, we co-transfected cells with CA-JNK1 or DN-JNK1, BNIP3 and Ub and then conducted a Co-IP assay. We were pleasantly surprised to find that CA-JNK1 significantly reduced the conjugation of ubiquitin to BNIP3 (Fig. 6f). Altogether, our results suggest that JNK1/2 improves the stability of BNIP3 by preventing its degradation via the ubiquitin-proteasome pathway. Thus, we propose that phosphorylation at the Ser 60/Thr 66 residue by JNK1/2 impedes the degradation of BNIP3 via the ubiquitin-proteasome pathway and that the stabilized BNIP3 promotes mitophagy via enhanced interaction with LC3.

DISCUSSION

Here we demonstrate that phosphorylation and ubiquitination of BNIP3 are crucial for the regulation of mitophagy. BNIP3 phosphorylation at Ser 60/Thr 66 by activated JNK1/2 under

moderate hypoxia conditions (10% O₂ or early stages of 0.3% O₂) blocks BNIP3 degradation via the ubiquitin-proteasome pathway, and then the stabilized and activated BNIP3 recruits LC3, thereby promoting mitophagy; however, JNK1/2 inactivation results in BNIP3 dephosphorylation by PP1/2A under severe hypoxia conditions (late stages of 0.3% O₂) and therefore accelerates BNIP3 proteasomal degradation, which impairs the induction of mitophagy (Fig. 7).

Regulation of mitophagy under hypoxia is crucial for cell fate and is related to whether cells adapt to hypoxia. BNIP3 is a mitophagy receptor that mediates mitophagy and is also a hypoxia-responsive protein that is highly upregulated under hypoxia, but the posttranslational modification of BNIP3 to regulate mitophagy under hypoxia remains a challenging problem. Early studies showed that BNIP3 could be phosphorylated in rat primary cultured cardiomyocytes and some cell lines [40, 41]. Recent studies further demonstrate that phosphorylation of BNIP3/BNIP3L plays an important role in mitophagy induction [16, 18, 19]. Notably, the phosphorylation of BNIP3 at Ser 17/24 flanking the LIR has been shown to enhance its binding to LC3 and promote mitophagy [16]. Recently, it has been reported that ULK1 phosphorylates BNIP3 on Ser 17, which promotes mitophagy and BNIP3 protein stability [17]. Such a modulatory mode for BNIP3 supports our work to a certain extent. But so far, little is known about the roles and regulatory mechanism of BNIP3 phosphorylation under pathological or physiological conditions.

In this study, we found phosphorylation of BNIP3 was dynamically regulated under hypoxia. Based on mass spectrum database and site-mutants screening, we uncovered that phosphorylation of BNIP3 at S60/T66 was regulated by hypoxia. To our surprise, the phosphorylation of BNIP3 at Ser 60/Thr 66 is not only critical for mitophagy induction (strengthen the interaction between BNIP3 and LC3, Fig. 2g and Supplementary Fig. S2c),

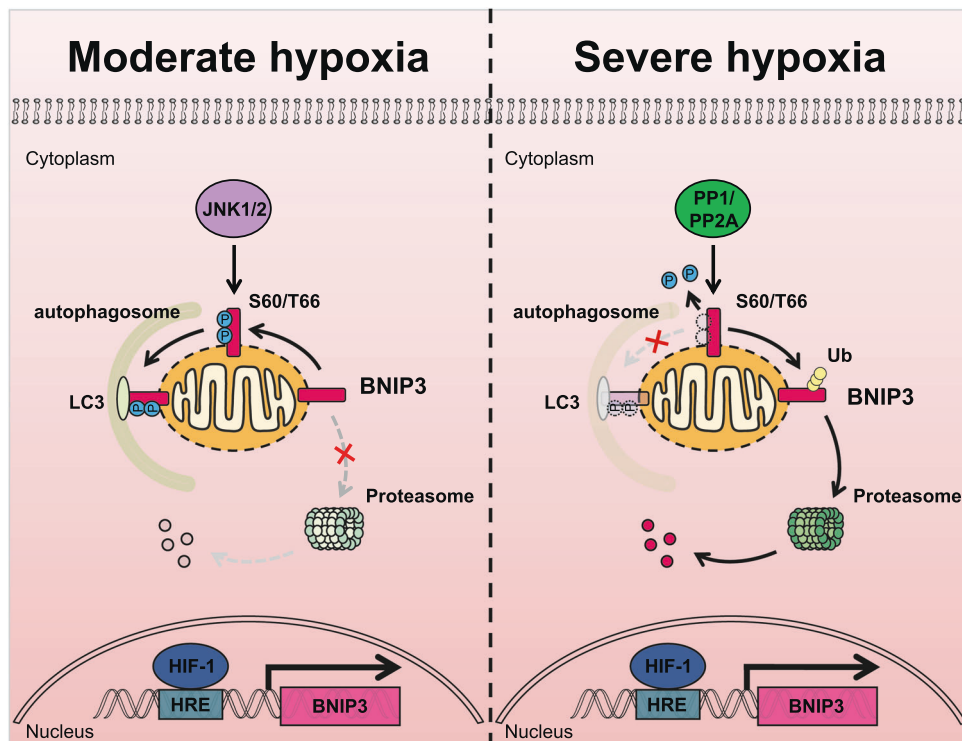


Fig. 7 The hypothetical mechanism of BNIP3 phosphorylation-mediated mitophagy under hypoxia. In response to moderate hypoxia (10% O₂ or early stages of 0.3% O₂), a generous amount of BNIP3 is phosphorylated at S60/T66 by JNK1/2, which blocks the conjugation of ubiquitin (Ub) to BNIP3, inducing mitophagy activation. In severe hypoxia (late stages of 0.3% O₂), JNK1/2 is inactivated and BNIP3 is dephosphorylated by PP1 or PP2A, which leads to the recruitment of ubiquitin to BNIP3 and its degradation via the ubiquitin-proteasome pathway, suppressing the induction of mitophagy.

but also for autophagy induction (increase the ratio of LC3-II/I and the formation of LC3 puncta, Fig. 2f, g and Supplementary Fig. S2e). However, we found that phosphorylation of BNIP3 at Ser 60/Thr 66 is not involved in regulation of BNIP3/BCL-2 interaction, which is a canonical pathway for autophagy induction (Supplementary Fig. S2b). We speculate that there may be another pathway to regulate autophagy mediated by phosphorylation of BNIP3 at Ser 60/Thr 66. Moreover, Ser 60/Thr 66 are located in the PEST domain of BNIP3, which has been reported related to the stability of BNIP3 [42]. Our results show that BNIP3 phosphorylation at the Ser 60/Thr 66 residue hinders its degradation via the ubiquitin-proteasome pathway and improves its stability. These results explain that BNIP3 phosphorylation at Ser 60/Thr 66 enhances the induction of autophagy and mitophagy probably through regulating the degradation of BNIP3.

Screening via inhibitor and siRNA, we next identified JNK1/2 as the kinase of BNIP3 at Ser 60/Thr 66, which contributes to induction of mitophagy by enhancing the BNIP3-LC3 interaction. Since JNK also activates BCL-2, which facilitates the dissociation of Beclin-1 from BCL-2 [46, 47], we explored whether phosphorylation at Ser 60/Thr 66 by JNK1/2 is involved in the interaction of BNIP3 with BCL-2. Unfortunately, we found that phosphorylation of BNIP3 at Ser 60/Thr 66 is not associated with binding of BCL-2, as the S60/T66A mutant did not alter the interaction of BNIP3 with BCL-2 (Supplementary Fig. S2b). However, this result does not rule out the possibility that other phosphorylation sites participate in the binding of BNIP3 to BCL-2. In addition, we have not further clarified how JNK is activated under hypoxia. But previous studies have shown that short-term hypoxia or ischemia can activate JNK, and long-term hypoxia or ischemia can lead to JNK inactivation [48, 49]. In addition, we identified PP1 and PP2A as BNIP3 phosphatases, which block mitophagy by dephosphorylation of BNIP3. Dephosphorylation of BNIP3 by PP1/2A not only plays a negative regulatory role in the induction of mitophagy but also in the stability of BNIP3. Especially, the degradation of BNIP3 through the ubiquitin-proteasome pathway was significantly accelerated by dephosphorylation. It is a pity that we did not find an E3 ligase for BNIP3 that regulates its proteasomal degradation. Although it is not clear whether the above kinases and phosphatases can directly regulate the function of proteasome, it is interesting that the stability of several BCL-2 family members has been reported to be closely related to their phosphorylation [50–54].

In conclusion, we provide evidence that BNIP3 phosphorylation level is more crucial for the induction of mitophagy than its total protein level, and that JNK1/2 and PP1/2A oppositely regulate the phosphorylation and stability of BNIP3 in response to different hypoxia. Future identification of an E3 ligase for BNIP3 and its regulation under hypoxia will be of great significance for revealing the comprehensive functions of BNIP3. Further study on the biological significance of coordinated regulation of BNIP3 by JNK1/2 and PP1/2A under hypoxic conditions could provide insight into therapeutic strategies against hypoxia-related diseases.

DATA AVAILABILITY

The datasets generated during and/or analyzed during the current study are available from the corresponding author on reasonable request.

REFERENCES

- Scherz-Shouval R, Elazar Z. Regulation of autophagy by ROS: physiology and pathology. *Trends Biochem Sci.* 2011;36:30–8.
- Kubli DA, Gustafsson AB. Mitochondria and mitophagy: the yin and yang of cell death control. *Circ Res.* 2012;111:1208–21.
- Ashrafi G, Schwarz TL. The pathways of mitophagy for quality control and clearance of mitochondria. *Cell Death Differ.* 2013;20:31–42.
- Marino G, Niso-Santano M, Baehrecke EH, Kroemer G. Self-consumption: the interplay of autophagy and apoptosis. *Nat Rev Mol Cell Biol.* 2014;15:81–94.
- Palikaras K, Lionaki E, Tavernarakis N. Mechanisms of mitophagy in cellular homeostasis, physiology and pathology. *Nat Cell Biol.* 2018;20:1013–22.
- Youle RJ, Narendra DP. Mechanisms of mitophagy. *Nat Rev Mol Cell Biol.* 2011;12:9–14.
- Dikic I, Elazar Z. Mechanism and medical implications of mammalian autophagy. *Nat Rev Mol Cell Biol.* 2018;19:349–64.
- Khaminets A, Behl C, Dikic I. Ubiquitin-dependent and independent signals in selective autophagy. *Trends Cell Biol.* 2016;26:6–16.
- Pickrell AM, Youle RJ. The roles of PINK1, parkin, and mitochondrial fidelity in Parkinson's disease. *Neuron* 2015;85:257–73.
- Hamacher-Brady A, Brady NR. Mitophagy programs: mechanisms and physiological implications of mitochondrial targeting by autophagy. *Cell Mol Life Sci.* 2016;73:775–95.
- Liu L, Sakakibara K, Chen Q, Okamoto K. Receptor-mediated mitophagy in yeast and mammalian systems. *Cell Res.* 2014;24:787–95.
- Kirkin V, Rogov W. A diversity of selective autophagy receptors determines the specificity of the autophagy pathway. *Mol Cell.* 2019;76:268–85.
- Wang L, Qi H, Tang Y, Shen HM. Post-translational modifications of key machinery in the control of mitophagy. *Trends Biochem Sci.* 2020;45:58–75.
- Pickles S, Vigié P, Youle RJ. Mitophagy and quality control mechanisms in mitochondrial maintenance. *Curr Biol.* 2018;28:R170–r185.
- Liu L, Li Y, Chen Q. The emerging role of FUNDC1-mediated mitophagy in cardiovascular diseases. *Front Physiol.* 2021;12:807654.
- Zhu Y, Massen S, Terenzio M, Lang V, Chen-Lindner S, Eils R, et al. Modulation of serines 17 and 24 in the LC3-interacting region of Bnip3 determines pro-survival mitophagy versus apoptosis. *J Biol Chem.* 2013;288:1099–113.
- Poole LP, Bock-Hughes A, Berardi DE, Macleod KF. ULK1 promotes mitophagy via phosphorylation and stabilization of BNIP3. *Sci Rep.* 2021;11:20526.
- Rogov W, Suzuki H, Marinkovic M, Lang V, Kato R, Kawasaki M, et al. Phosphorylation of the mitochondrial autophagy receptor Nix enhances its interaction with LC3 proteins. *Sci Rep.* 2017;7:1131.
- Yuan Y, Zheng Y, Zhang X, Chen Y, Wu X, Wu J, et al. BNIP3L/NIX-mediated mitophagy protects against ischemic brain injury independent of PARK2. *Autophagy* 2017;13:1754–66.
- Marinkovic M, Sprung M, Novak I. Dimerization of mitophagy receptor BNIP3L/NIX is essential for recruitment of autophagic machinery. *Autophagy* 2021;17:1232–43.
- da Silva Rosa SC, Martens MD, Field JT, Nguyen L, Kereliuk SM, Hai Y, et al. BNIP3L/Nix-induced mitochondrial fission, mitophagy, and impaired myocyte glucose uptake are abrogated by PRKA/PKA phosphorylation. *Autophagy* 2021;17:2257–72.
- Chen G, Ray R, Dubik D, Shi L, Cizeau J, Bleackley RC, et al. The E1B 19K/Bcl-2-binding protein Nip3 is a dimeric mitochondrial protein that activates apoptosis. *J Exp Med.* 1997;186:1975–83.
- Yasuda M, Theodorakis P, Subramanian T, Chinnadurai G. Adenovirus E1B-19K/BCL-2 interacting protein BNIP3 contains a BH3 domain and a mitochondrial targeting sequence. *J Biol Chem.* 1998;273:12415–21.
- Bruick RK. Expression of the gene encoding the proapoptotic Nip3 protein is induced by hypoxia. *Proc Natl Acad Sci USA.* 2000;97:9082–7.
- Guo K, Searfoss G, Krolkowski D, Pagnoni M, Franks C, Clark K, et al. Hypoxia induces the expression of the pro-apoptotic gene BNIP3. *Cell Death Differ.* 2001;8:367–76.
- Sowter HM, Ratcliffe PJ, Watson P, Greenberg AH, Harris AL. HIF-1-dependent regulation of hypoxic induction of the cell death factors BNIP3 and NIX in human tumors. *Cancer Res.* 2001;61:6669–73.
- Diwan A, Krenz M, Syed FM, Wansapura J, Ren X, Koesters AG, et al. Inhibition of ischemic cardiomyocyte apoptosis through targeted ablation of Bnip3 restrains postinfarction remodeling in mice. *J Clin Invest.* 2007;117:2825–33.
- Zhang H, Bosch-Marce M, Shimoda LA, Tan YS, Baek JH, Wesley JB, et al. Mitochondrial autophagy is an HIF-1-dependent adaptive metabolic response to hypoxia. *J Biol Chem.* 2008;283:10892–903.
- Bellot G, Garcia-Medina R, Gounon P, Chiche J, Roux D, Pouyssegur J, et al. Hypoxia-induced autophagy is mediated through hypoxia-inducible factor induction of BNIP3 and BNIP3L via their BH3 domains. *Mol Cell Biol.* 2009;29:2570–81.
- Chourasia AH, Tracy K, Frankenberger C, Boland ML, Sharifi MN, Drake LE, et al. Mitophagy defects arising from Bnip3 loss promote mammary tumor progression to metastasis. *EMBO Rep.* 2015;16:1145–63.
- Ney PA. Mitochondrial autophagy: Origins, significance, and role of BNIP3 and NIX. *Biochim Biophys Acta.* 2015;1853:2775–83.
- Hanna RA, Quinsay MN, Orogo AM, Giang K, Rikka S, Gustafsson AB. Microtubule-associated protein 1 light chain 3 (LC3) interacts with Bnip3 protein to selectively remove endoplasmic reticulum and mitochondria via autophagy. *J Biol Chem.* 2012;287:19094–104.
- Ma X, Godar RJ, Liu H, Diwan A. Enhancing lysosome biogenesis attenuates BNIP3-induced cardiomyocyte death. *Autophagy* 2012;8:297–309.

34. Xu G, Li T, Chen J, Li C, Zhao H, Yao C, et al. Autosomal dominant retinitis pigmentosa-associated gene PRPF8 is essential for hypoxia-induced mitophagy through regulating ULK1 mRNA splicing. *Autophagy* 2018;14:1818–30.
35. Wang J, Tang R, Lv M, Wang Q, Zhang X, Guo Y, et al. Defective anchoring of JNK1 in the cytoplasm by MKK7 in Jurkat cells is associated with resistance to Fas-mediated apoptosis. *Mol Biol Cell*. 2011;22:117–27.
36. Millhorn DE, Conforti L, Beitner-Johnson D, Zhu W, Raymond R, Filisko T, et al. Regulation of ionic conductances and gene expression by hypoxia in an oxygen sensitive cell line. *Adv Exp Med Biol*. 1996;410:135–42.
37. Katayama H, Kogure T, Mizushima N, Yoshimori T, Miyawaki A. A sensitive and quantitative technique for detecting autophagic events based on lysosomal delivery. *Chem Biol*. 2011;18:1042–52.
38. Sun N, Yun J, Liu J, Malide D, Liu C, Rovira II, et al. Measuring in vivo mitophagy. *Mol Cell*. 2015;60:685–96.
39. Yamashita SI, Jin X, Furukawa K, Hamasaki M, Nezu A, Otera H, et al. Mitochondrial division occurs concurrently with autophagosome formation but independently of Drp1 during mitophagy. *J Cell Biol*. 2016;215:649–65.
40. Graham RM, Thompson JW, Wei J, Bishopric NH, Webster KA. Regulation of Bnip3 death pathways by calcium, phosphorylation, and hypoxia-reoxygenation. *Antioxid Redox Signal*. 2007;9:1309–15.
41. Mellor HR, Rouschop KM, Wigfield SM, Wouters BG, Harris AL. Synchronised phosphorylation of BNIP3, Bcl-2 and Bcl-xL in response to microtubule-active drugs is JNK-independent and requires a mitotic kinase. *Biochem Pharm*. 2010;79:1562–72.
42. Cizeau J, Ray R, Chen G, Gietz RD, Greenberg AH. The *C. elegans* orthologue ceBNIP3 interacts with CED-9 and CED-3 but kills through a BH3- and caspase-independent mechanism. *Oncogene* 2000;19:5453–63.
43. Shi Y. Serine/threonine phosphatases: mechanism through structure. *Cell* 2009;139:468–84.
44. Chen G, Han Z, Feng D, Chen Y, Chen L, Wu H, et al. A regulatory signaling loop comprising the PGAM5 phosphatase and CK2 controls receptor-mediated mitophagy. *Mol Cell*. 2014;54:362–77.
45. Kanki T, Kurihara Y, Jin X, Goda T, Ono Y, Aihara M, et al. Casein kinase 2 is essential for mitophagy. *EMBO Rep*. 2013;14:788–94.
46. Wei Y, Patingre S, Sinha S, Bassik M, Levine B. JNK1-mediated phosphorylation of Bcl-2 regulates starvation-induced autophagy. *Mol Cell*. 2008;30:678–88.
47. Wei Y, Sinha S, Levine B. Dual role of JNK1-mediated phosphorylation of Bcl-2 in autophagy and apoptosis regulation. *Autophagy* 2008;4:949–51.
48. Laderoute KR, Mendonca HL, Calaoagan JM, Knapp AM, Giaccia AJ, Stork PJ. Mitogen-activated protein kinase phosphatase-1 (MKP-1) expression is induced by low oxygen conditions found in solid tumor microenvironments. A candidate MKP for the inactivation of hypoxia-inducible stress-activated protein kinase/c-Jun N-terminal protein kinase activity. *J Biol Chem*. 1999;274:12890–7.
49. Zhou G, Golden T, Aragon IV, Honkanen RE. Ser/Thr protein phosphatase 5 inactivates hypoxia-induced activation of an apoptosis signal-regulating kinase 1/ MKK-4/JNK signaling cascade. *J Biol Chem*. 2004;279:46595–605.
50. Harley ME, Allan LA, Sanderson HS, Clarke PR. Phosphorylation of Mcl-1 by CDK1-cyclin B1 initiates its Cdc20-dependent destruction during mitotic arrest. *EMBO J*. 2010;29:2407–20.
51. Inuzuka H, Shaik S, Onoyama I, Gao D, Tseng A, Maser RS, et al. SCF(FBW7) regulates cellular apoptosis by targeting MCL1 for ubiquitylation and destruction. *Nature* 2011;471:104–9.
52. Wertz IE, Kusam S, Lam C, Okamoto T, Sandoval W, Anderson DJ, et al. Sensitivity to antitubulin chemotherapeutics is regulated by MCL1 and FBW7. *Nature* 2011;471:110–4.
53. Leboucher GP, Tsai YC, Yang M, Shaw KC, Zhou M, Veenstra TD, et al. Stress-induced phosphorylation and proteasomal degradation of mitofusin 2 facilitates mitochondrial fragmentation and apoptosis. *Mol Cell*. 2012;47:547–57.
54. Moustafa-Kamal M, Gamache I, Lu Y, Li S, Teodoro JG. BimEL is phosphorylated at mitosis by Aurora A and targeted for degradation by β TrCP1. *Cell Death Differ*. 2013;20:1393–403.

ACKNOWLEDGEMENTS

We thank Prof. Q. Xia and T. Zhou (State Key Laboratory of Proteomics, Beijing) for providing the pXJ40-HA, pXJ40-Myc-Ub, pEGFP-C1-LC3B, pEGFP-C1-PPP1CA, and pEGFP-C1-PPP1CC plasmids and Prof. J.-Y. Zhang (Beijing Institute of Basic Medical Sciences, Beijing) for providing the pSR α -HA-MKK7-JNK1 (JNK1^{CA}) and pSR α -HA-JNK1-APF (JNK1^{DN}) plasmids.

AUTHOR CONTRIBUTIONS

L.Y.W., L.L.Z., H.T.W., and M.F. designed and supervised the project. L.Y.W. and Y.L.H. designed and performed the majority of the experiments. Y.L.H. and J.L. contributed to the Western blotting. Y.L.H., J.L., S.H.G., M.Z., and Y.C. contributed to the immunofluorescence analysis. X.C. and T.Z. helped to prepare cell lines and reagents. Y.Q.Z. provided technical support. L.Y.W. and Y.L.H. interpreted the data and wrote the manuscript, with the help of all the authors.

FUNDING

This work was supported by grants from the National Natural Science Foundation of China (31271211, 31771321, and 81971781 to L.Y.W. and 32171148 to H.T.W.), the Key Program of National Nature Sciences Foundation of China (81430044 to L.L.Z.), the National Key Research and Development Program of China (2021ZD0202500 and 2021YFA1101801 to H.T.W. and 2021YFA1101800 to L.L.Z.), and the National Basic Research Program of China (2011CB910800 to L.L.Z. and 2012CB518200 to M.F.).

COMPETING INTERESTS

The authors declare no competing interests.

ADDITIONAL INFORMATION

Supplementary information The online version contains supplementary material available at <https://doi.org/10.1038/s41419-022-05418-z>.

Correspondence and requests for materials should be addressed to Ming Fan, Hai-Tao Wu, Ling-Ling Zhu or Li-Ying Wu.

Reprints and permission information is available at <http://www.nature.com/reprints>

Publisher's note Springer Nature remains neutral with regard to jurisdictional claims in published maps and institutional affiliations.



Open Access This article is licensed under a Creative Commons Attribution 4.0 International License, which permits use, sharing, adaptation, distribution and reproduction in any medium or format, as long as you give appropriate credit to the original author(s) and the source, provide a link to the Creative Commons license, and indicate if changes were made. The images or other third party material in this article are included in the article's Creative Commons license, unless indicated otherwise in a credit line to the material. If material is not included in the article's Creative Commons license and your intended use is not permitted by statutory regulation or exceeds the permitted use, you will need to obtain permission directly from the copyright holder. To view a copy of this license, visit <http://creativecommons.org/licenses/by/4.0/>.

© The Author(s) 2022